

A new algorithm for surface tension model in moving particle methods

Shuai Zhang^{*,†}, Koji Morita, Kenji Fukuda and Noriyuki Shirakawa

Department of Applied Quantum Physics and Nuclear Engineering, Kyushu University, Fukuoka, Japan

SUMMARY

A new algorithm for the surface tension model was developed for moving particle methods. The algorithm is based on the link-list search algorithm and the continuum surface tension (CST) model. The developed algorithm with the CST model was implemented to a kind of moving particle approach, the finite volume particle (FVP) method. The FVP method with the new algorithm was tested by oscillatory behaviour of a two-dimensional droplet. The oscillatory period agrees well with analytical one, and the transient shape of the droplet is also in good agreement with that obtained by other numerical methods. The droplet impact on a liquid surface was also studied using the new algorithm. The deposition and splashing phenomena were clearly reproduced. Simulated spread radius of the splashing phenomena was consistent with a power law. Copyright © 2007 John Wiley & Sons, Ltd.

Received 22 August 2006; Revised 15 November 2006; Accepted 24 November 2006

KEY WORDS: moving particle methods; finite volume particle (FVP) method; Continuum surface tension (CST) model; droplet impact

1. INTRODUCTION

Surface tension force is very important in fluid dynamics, especially in multiphase and free surface flow problems. The continuum surface tension (CST) model [1] has been developed and widely applied to calculate the surface tension force in Eulerian methods. Though it was originally proposed for grid methods, the CST model has been also applied in moving particle methods nowadays, for example, in the smoothed particle hydrodynamics (SPH) method [2] and the moving particle semi-implicit (MPS) method [3]. In the MPS method, the unit normal and curvature of the interfaces are estimated from the particle number density. However, it is difficult to precisely estimate the

^{*}Correspondence to: Shuai Zhang, Department of Applied Quantum Physics and Nuclear Engineering, Kyushu University, Fukuoka, Japan.

[†]E-mail: zhang@nucl.kyushu-u.ac.jp

Contract/grant sponsor: Ministry of Education, Culture, Sports, Science and Technology

curvature near the surface when particle arrangement is in disorder, especially in three-dimensional cases.

It is worth to note that the surface tension force was successfully simulated in a hybrid particle-mesh combined method [4]. In this method, each moving particle is assumed to hold a fixed volume. The surface tension force is calculated for each moving particle using the same model as that in the MPS method. Then the momentum caused by the surface tension and other external forces are extrapolated from moving particles to background cells according to the overlaid volume between particles and mesh cells. After that, the pressure will be estimated on the background mesh with the incompressible constraint. Finally, the momentum is transferred from background mesh to moving particles. With this combined method, the unnaturally estimated surface tension force caused by the disorder of moving particles can be smoothed out on the background mesh.

Recently, a new fully Lagrangian moving particle method, named the finite volume particle (FVP) method, was developed for incompressible fluids with free surface [5]. In the FVP method, assuming that one particle occupies a finite volume, governing equations are discretized using the approach of the finite volume method. The solution scheme is based on the pressure implicit with splitting of operators (PISO) algorithm. The discretized matrix equations are solved using the incomplete Cholesky conjugate gradient (ICCG) algorithm. Compared to the MPS method, which is also a fully Lagrangian moving particle method for incompressible fluids, the FVP method can estimate the pressure more reasonably and thus numerically more stable [5]. In addition, this method needs no special treatment for moving particles on the free surface.

Since each FVP particle occupies a finite volume, it is natural to implement the same particle-mesh combined algorithm as mentioned above. In the present study, a temporal background mesh is automatically built up with the implementation of the link-list search algorithm [6]. The mass of each cell is extrapolated from moving particles, based on their overlaid volumes. Thereafter, the surface tension force can be easily estimated on the background mesh using the CST model. Finally, the surface tension force for each moving particle is extrapolated from the background mesh according to their overlaid volumes.

In this new algorithm for the surface tension model, the mass and momentum between moving particles and the background mesh are conserved. The extrapolated mass field of the background mesh is always smooth in the implementation of this algorithm. Correspondingly, the curvature on the interface can be estimated precisely and stably using the CST model.

Two benchmark calculations will be performed to verify the proposed algorithm for the surface tension model in moving particle methods. One is the oscillation of a liquid droplet; the other is the impact of a liquid droplet on a liquid surface. Simulated results will be compared with analytical ones and those obtained by other numerical methods.

2. OVERVIEW OF FVP METHOD

2.1. Governing equations

With the Gauss's law, governing equations for incompressible flows, namely the mass and momentum conservation equations are rearranged as follows:

$$\oint_S \mathbf{u} \cdot \mathbf{n} ds = 0 \quad (1)$$

$$\frac{D}{Dt} \int_V \mathbf{u} dV = -\frac{1}{\rho} \oint_s p \mathbf{n} ds + \frac{1}{\rho} \oint_s \mu \nabla \mathbf{u} ds + \mathbf{F} \quad (2)$$

where \mathbf{F} is the external force.

2.2. Discretization method

As shown in Figure 1, the control volume of one moving particle is assumed as a circle in two-dimensional simulations [5]:

$$\pi R^2 = (\Delta l)^2 \quad (3)$$

where R and Δl are radius of particle control volume and initial particle distance, respectively. Then Equation (2) can be arranged as

$$\frac{D\mathbf{u}}{Dt} = -\lim_{R \rightarrow 0} \frac{1}{\rho \pi R^2} \oint_s p \mathbf{n} ds + \lim_{R \rightarrow 0} \frac{1}{\rho \pi R^2} \oint_s \mu \frac{\partial \mathbf{u}}{\partial n} ds + \mathbf{F} \quad (4)$$

The interaction surface of particle j to particle i , $\Delta \mathbf{S}_{ij}$, is estimated as [5]

$$\Delta \mathbf{S}_{ij} = 2R\theta_{ij} \mathbf{n} \quad (5)$$

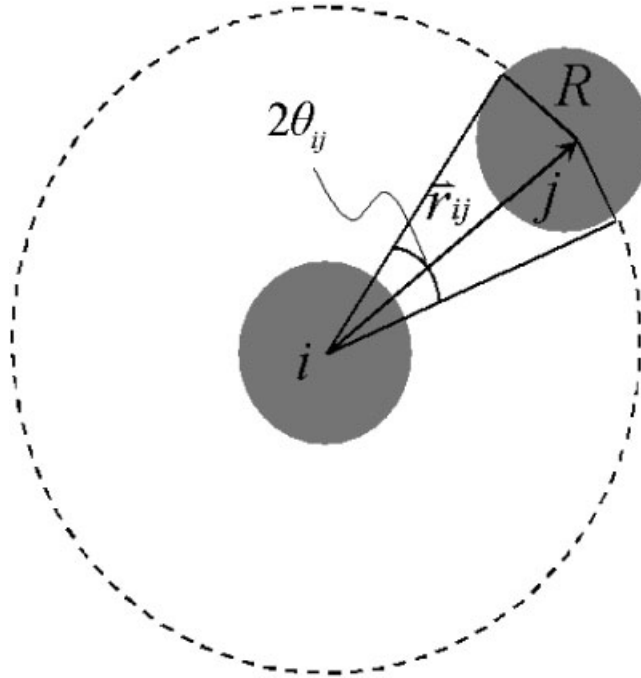


Figure 1. Interaction between two particles.

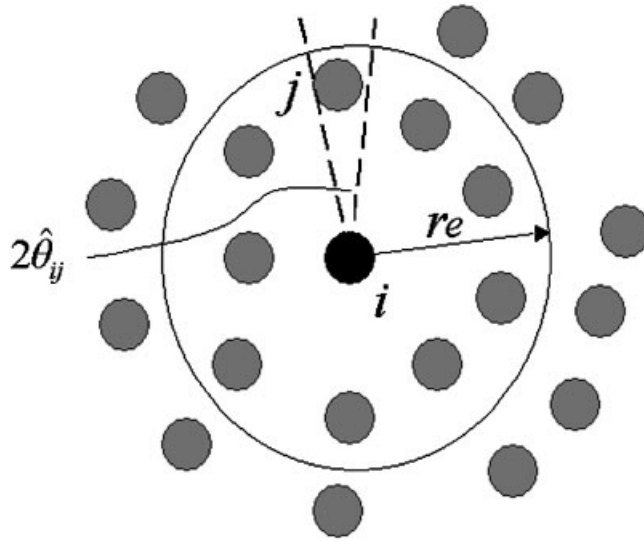


Figure 2. Interaction between two particles within a limited support domain.

where \mathbf{n} is the unit vector of distance between two particles

$$\mathbf{n} = \mathbf{r}_{ij} / |\mathbf{r}_{ij}| = (\mathbf{r}_j - \mathbf{r}_i) / |\mathbf{r}_{ij}| \quad (6)$$

and the parameter θ_{ij} is defined as

$$\theta_{ij} = \sin^{-1}(R/|\mathbf{r}_{ij}|) \quad (7)$$

In order to define a compact interaction domain, the following treatment is necessary [5]:

$$\hat{\theta}_{ij} = \sin^{-1}(R/|\mathbf{r}_{ij}|) - \sin^{-1}(R/r_e) \quad (8)$$

where r_e is the cut-off radius, as shown in Figure 2. Thereafter, the interaction surface will be normalized as

$$\Delta \mathbf{S}_{ij} = \begin{cases} 2\alpha R \hat{\theta}_{ij} \mathbf{n}, & \hat{\theta}_{ij} \geq 0 \\ 0, & \hat{\theta}_{ij} < 0 \end{cases} \quad (9)$$

where parameter α is

$$\alpha = \pi / \sum_{j=1, j \neq i}^n \hat{\theta}_{ij} \quad (10)$$

From above on, Equation (4) is discretized as

$$\left(\frac{D\mathbf{u}}{Dt} \right)_i = - \frac{1}{\rho\pi R^2} \sum_{j=1, j \neq i}^n \left(p_j + \frac{p_j - p_i}{|\mathbf{r}_{ij}|} R \right) \Delta \mathbf{S}_{ij} + \frac{\mu}{\rho\pi R^2} \sum_{j=1, j \neq i}^n \frac{\mathbf{u}_j - \mathbf{u}_i}{|\mathbf{r}_{ij}|} |\Delta \mathbf{S}_{ij}| + \mathbf{F} \quad (11)$$

It is worth to note that the pressure gradient and the velocity Laplacian terms of Equation (11) are of first-order accuracy.

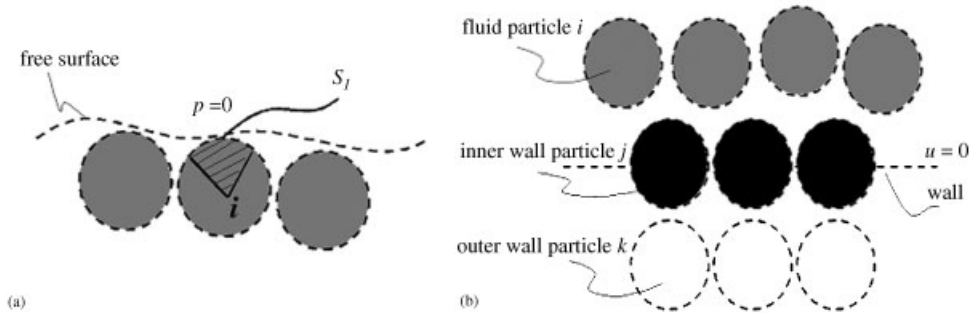


Figure 3. Boundary treatments in the FVP method: (a) free surface and (b) wall boundary.

2.3. Boundary conditions

In the FVP method, there are two kinds of boundary conditions, wall and free surface boundary conditions. As seen in Figure 3(a), \mathbf{S}_i is referred to the surface of one particle on the free surface:

$$\mathbf{S}_i = -\sum \Delta \mathbf{S}_{ij} \quad (12)$$

$$|\mathbf{S}_i| = 2\pi R - \sum |\Delta \mathbf{S}_{ij}| \quad (13)$$

Zero pressure and velocity gradients are set on the free surface.

Figure 3(b) shows the wall boundary treatments. The pressures of inner wall particles should be calculated together with fluid particles. A static pressure head is added for the outer wall particles as [5]

$$p_k = p_j + \rho g h_{kj} \quad (14)$$

where h_{kj} is the distance between particles j and k in the direction of gravity. According to the non-slip boundary condition, zero velocity is kept on the inner wall particles with the second-order accuracy as

$$\mathbf{u}_k = -\mathbf{u}_i \frac{h_i}{h_k} \quad (15)$$

where h_i and h_k are the distances for particles i and k away from the wall.

2.4. Pressure Poisson equation

Combining Equations (1) and (2), a pressure Poisson equation can be obtained:

$$\frac{1}{\rho} \oint_S (\nabla p) \cdot \mathbf{n} ds = \frac{1}{\Delta t} \int_V (\nabla \cdot \mathbf{u}) dV \quad (16)$$

In the FVP method, Equation (16) is discretized as

$$\begin{aligned} & \frac{1}{\rho} \sum_{j=1, j \neq i}^n \frac{p_j - p_i}{|\mathbf{r}_{ij}|} |\Delta \mathbf{S}_{ij}| + \frac{p_{\text{free}} - p_i}{\rho R} |\mathbf{S}_1| \\ &= \frac{1}{\Delta t} \sum_{j=1, j \neq i}^n \left(\mathbf{u}_i + \frac{\mathbf{u}_j - \mathbf{u}_i}{|\mathbf{r}_{ij}|} R \right) \cdot \Delta \mathbf{S}_{ij} + \frac{1}{\Delta t} \left[\mathbf{u}_i + \left(\frac{\partial \mathbf{u}}{\partial n} \right)_{\text{free}} R \right] \cdot \mathbf{S}_1 \end{aligned} \quad (17)$$

where p_{free} and $(\partial \mathbf{u} / \partial n)_{\text{free}}$ are the values of pressure and velocity gradient on the free surface. In the present studies, both of them are set as zero. According to the boundary treatments, Equation (17) is rewritten as

$$\begin{aligned} & \frac{1}{\rho} \sum_{j=1, j \neq i}^n \frac{p_j - p_i}{|\mathbf{r}_{ij}|} |\Delta \mathbf{S}_{ij}| - \frac{p_i}{\rho R} |\mathbf{S}_1| \\ &= \frac{1}{\Delta t} \sum_{j=1, j \neq i}^n \left(\mathbf{u}_i + \frac{\mathbf{u}_j - \mathbf{u}_i}{|\mathbf{r}_{ij}|} R \right) \cdot \Delta \mathbf{S}_{ij} + \frac{1}{\Delta t} \mathbf{u}_i \cdot \mathbf{S}_1 \end{aligned} \quad (18)$$

2.5. Time integration

A fully implicit algorithm, the PISO algorithm [7], is incorporated in the FVP method, as seen in the Figure 4 [5]. In the present studies, the first-order forward time scheme was implemented. Firstly, particles move with assumed new-time velocities:

$$\mathbf{u}_i^* = \mathbf{u}_i^n \quad (19)$$

$$\mathbf{r}_i^* = \mathbf{r}_i^n + \mathbf{u}_i^* \Delta t \quad (20)$$

Thereafter, parameters, such as $\Delta \mathbf{S}_{ij}^*$, $|\Delta \mathbf{S}_{ij}^*|$, \mathbf{S}_1^* and $|\mathbf{S}_1^*|$ are temporally updated.

Secondly, the discretized momentum conservation and pressure Poisson equations

$$\mathbf{u}_i^* - \frac{\mu \Delta t}{\rho \pi R^2} \sum_{j=1, j \neq i}^n \frac{\mathbf{u}_j^* - \mathbf{u}_i^*}{|\mathbf{r}_{ij}^*|} |\Delta \mathbf{S}_{ij}^*| = \mathbf{u}_i^n - \frac{1}{\pi R^2} \sum_{j=1, j \neq i}^n \left(\hat{p}_i^* + \frac{\hat{p}_j^* - \hat{p}_i^*}{|\mathbf{r}_{ij}^*|} R \right) \Delta \mathbf{S}_{ij}^* + \mathbf{F} \Delta t \quad (21)$$

$$\sum_{j=1, j \neq i}^n \frac{\hat{p}_j^* - \hat{p}_i^*}{|\mathbf{r}_{ij}^*|} |\Delta \mathbf{S}_{ij}^*| - \frac{\hat{p}_i^*}{R} |\mathbf{S}_1^*| = \sum_{j=1, j \neq i}^n \left(\mathbf{u}_i^* + \frac{\mathbf{u}_j^* - \mathbf{u}_i^*}{|\mathbf{r}_{ij}^*|} R \right) \cdot \Delta \mathbf{S}_{ij}^* + \mathbf{u}_i^* \cdot \mathbf{S}_1^* \quad (22)$$

where

$$\hat{p}^* = \frac{\Delta t}{\rho} p^* \quad (23)$$

will be solved by the ICCG algorithm [8]. The temporal pressures and velocities will be obtained.

If solutions are satisfied, the temporal pressures and velocities are saved and particle positions will be updated with these new velocities; otherwise, they are used as assumed velocities and pressures and calculations go back to the first step to get temporal positions and parameters. In a

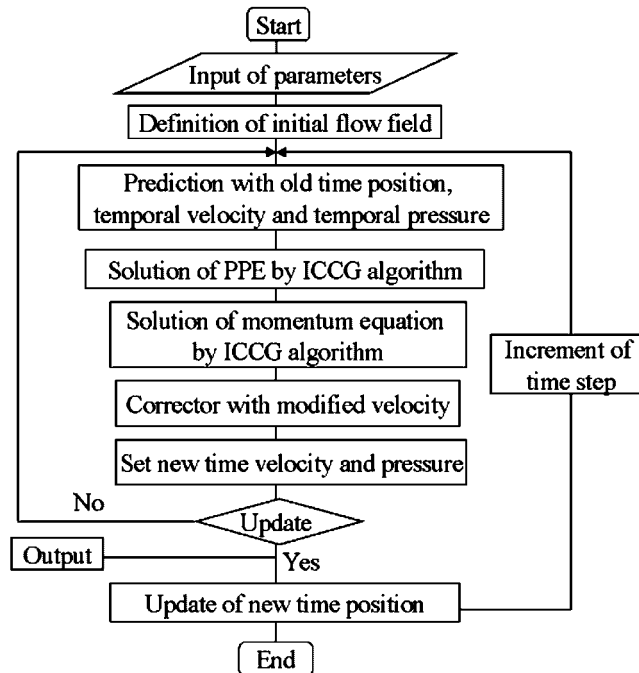


Figure 4. PISO algorithm applied in the FVP method.

turn, discretized Equations (21) and (22) will be solved. Iterations are generated in this way. In general, three iterations are enough for moderate errors.

The time increase will be taken according to the CFL condition as follows:

$$\max \left| \frac{(\mathbf{u}_j^n - \mathbf{u}_i^n) \cdot \mathbf{n} \Delta t}{|\mathbf{r}_{ij}^n|} \right| < \varepsilon \quad (24)$$

where ε is usually chosen as 0.2 [5]. Otherwise, the half value of old time increase is used.

3. A NEW ALGORITHM FOR SURFACE TENSION MODEL

3.1. Link-list search algorithm

In moving particle methods, each particle interacts with others in a compact support domain. In this case, it is necessary to apply some search algorithm to improve calculation efficiency. Since the FVP method has a spatially constant interaction length, the link-list search algorithm [6] is considered to be most appropriate for it. In the present study, a temporal grid is overlaid on the FVP calculation region when the link-list search algorithm is applied, as shown in Figure 5. The two-dimensional calculation region is separated into a set of square cells. In each cell, there are a certain number of particles in it. Particles interact with those in the same or neighbour cells. This

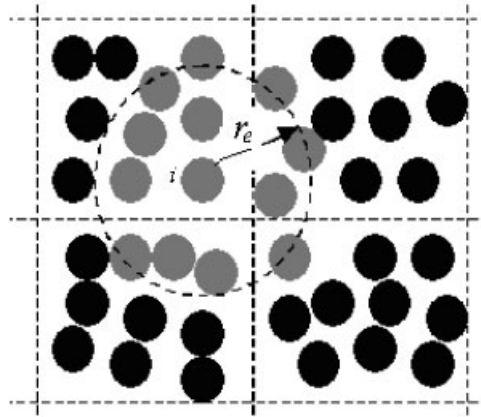


Figure 5. Schematic description of the link-list search algorithm.

search algorithm has been widely used in moving particle methods, such as the SPH and MPS methods.

3.2. Application of CSF model to FVP method

As we know, the CST model was originally developed for grid methods [1]. When it is applied in moving particle methods, the curvature and unit normal of the interface are usually estimated from particle number densities [3]. However, it is necessary to remove the singularity in the simulations caused by disorder in particle arrangements. In addition, when the calculation geometry is complicated, it is very difficult to estimate the curvature precisely.

In this study, by overlaying a temporal grid on the FVP calculation region, we apply the CST model to this temporal grid. Since the CST model evaluates the surface tension as a volume force, the surface tension force acting on a moving particle can be interpolated from the volume force of the grid according to the overlaid volume between particles and cells. As a result, the surface tension force acting on particles could be estimated reasonably with the standard CST model. The mathematical approach of this new algorithm for the surface tension model is explained as follows.

At first, the control volume of a particle is assumed as a square in two dimensions. As shown in Figure 6, the mass of cell is estimated by extrapolation from moving particles to cells as

$$m(ii, jj) = \frac{\rho \sum_{k=1}^N A_{ii,jj}^k}{\rho(\Delta L)^d} = \sum_{k=1}^N \frac{A_{ii,jj}^k}{(\Delta L)^d} \leq 1 \quad (25)$$

where m is the mass of one cell, d is number of dimensions, N is the number of particles in a cell, ΔL is the size of the background grid and $A_{ii,jj}^k$ is the volume that particle k overlapped with a cell (ii, jj) .

Then the surface tension force can be estimated using the CST model on the background grid [9]. Lastly, the surface tension of moving particles is extrapolated from the grid as

$$\mathbf{F}_i \cdot (\Delta L)^d = \left[\sum_{ii,jj} \frac{A_{ii,jj}^i}{(\Delta L)^d} \mathbf{F}_v(ii, jj) \right] \cdot (\Delta L)^d \quad (26)$$

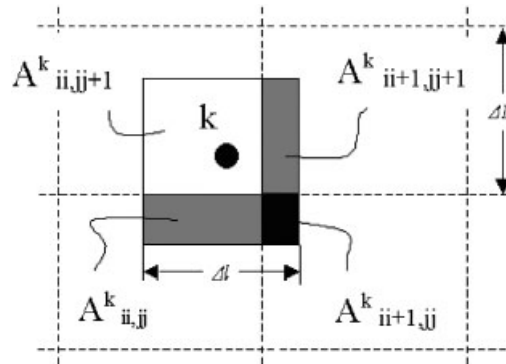


Figure 6. Extrapolation of cell mass from particles.

where \mathbf{F}_i and \mathbf{F}_v are the surface tension force of particles and cells, respectively. $A^i_{ii,jj}$ is the overlapped volume between particle i and cells. In the present study, ΔL is set to be $2.0\Delta l$.

4. NUMERICAL SIMULATIONS

4.1. Oscillation of square liquid droplet

Oscillation of a square liquid droplet is a good test case for the surface tension model, which has been simulated by both grid methods [1] and particle methods [2, 3]. In the present simulation, an ethanol square droplet with $\rho = 797.88 \text{ kg m}^{-3}$, $L = 0.075 \text{ m}$ and $\sigma = 0.02361 \text{ N m}^{-1}$ under surface tension was simulated with the proposed algorithm for the surface tension model. Gravity and other external forces were neglected. As shown in Figure 7, the initial particle array was 50×50 . The initial particle distance was 0.00125 m .

There is an analytic expression for the oscillation frequency of two-dimensional drop in zero gravity as [10]

$$w_n = \frac{(n^3 - n)\sigma}{\rho R_0^3} \quad (27)$$

where n is the mode number of oscillation ($n = 4$ in the present simulation) and R_0 is unperturbed radius of the droplet. According to Equation (27), the oscillation period of the ethanol droplet should be 1.30 s in the present case.

Simulation results are shown in Figures 8 and 9. In Figure 8, the transient shapes of the oscillatory liquid droplet are shown at four different time steps. Figure 8 shows the kinetic energy changes with time. From these two figures, it can be found that the simulated oscillation period was 1.31 s , which was a little larger than the analytical result. The shape of the ethanol droplet rotated by 45° at 0.57 and 1.78 s , while turned to the initial shape at 1.31 and 2.51 s . As can be seen in Figure 8, numerical dissipation eventually damps the oscillation and finally causes the droplet to approach an equilibrium spherical shape. The simulation results agree well with the analytical results and those obtained by others [1, 3].

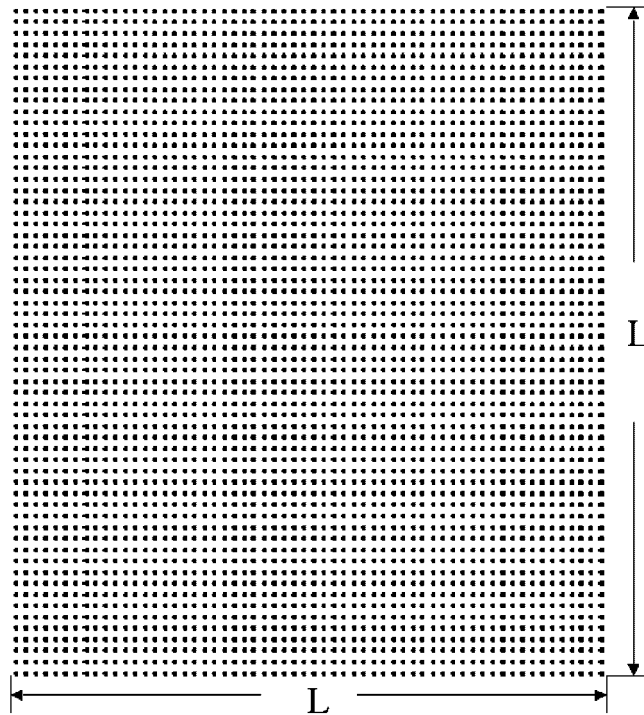


Figure 7. Initial particle arrangement of the square liquid droplet.

4.2. Droplet impact

A liquid droplet impact on a liquid surface can result in deposition or splashing of the surface, and, in some special cases, floating or bouncing of the droplet may also occur. There is a review of this complicated phenomenon [11]. Recently, the direct numerical simulation of this phenomenon has attracted attentions of many researchers [12, 13]. In this study, the FVP method with the proposed algorithm for the surface tension model was used to simulate this phenomenon.

The relevant non-dimensional parameters for this phenomenon are the Weber number and the Reynolds number as follow:

$$We = \frac{2\rho U^2 R}{\sigma} \quad (28)$$

$$Re = \frac{2\rho U R}{\mu} \quad (29)$$

where U is the velocity of the droplet at the instant of impact on a static liquid surface, R is the radius of the droplet, σ is the surface tension coefficient and μ is the dynamic viscosity. The non-dimensional time is measured by $2R/U$. Previous research has established an empirical relation, named as the Sommerfeld's law, for the crossover between spreading and deposition

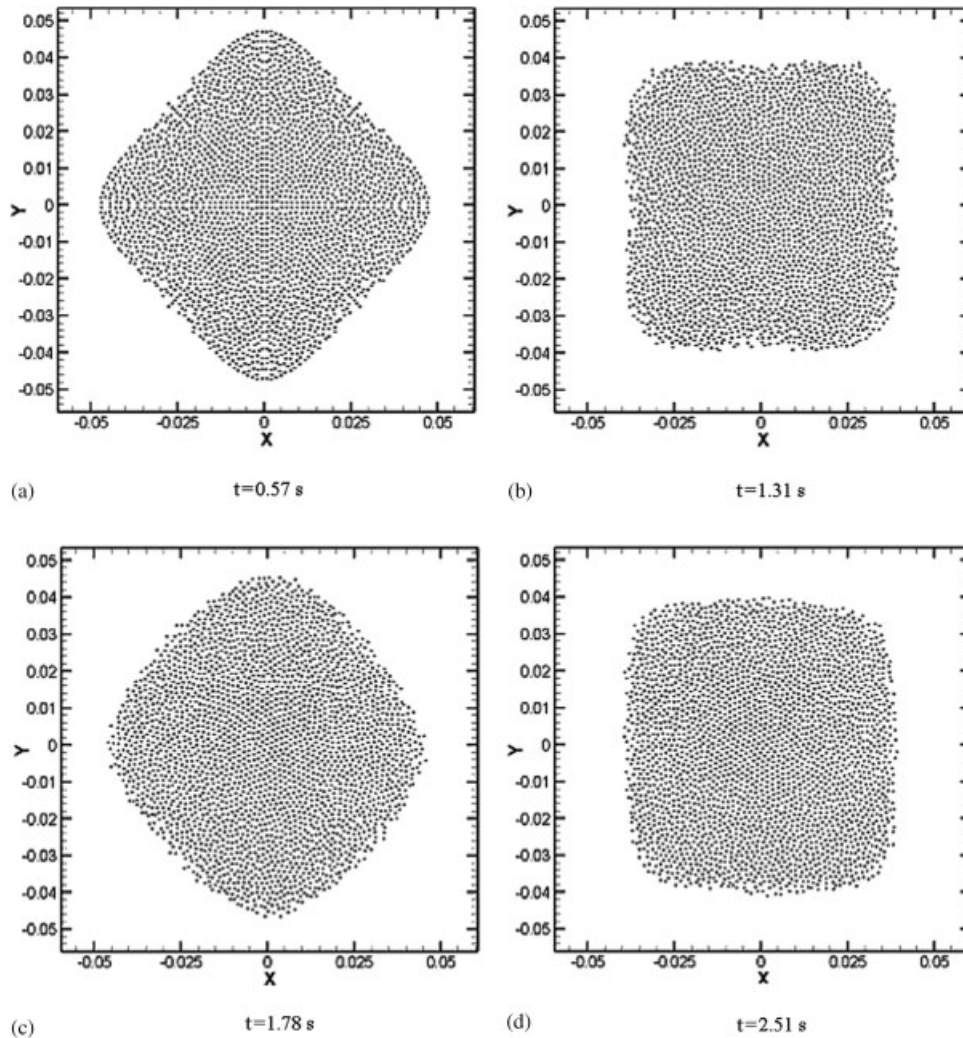


Figure 8. Simulated sequences of oscillation of the square ethanol droplet under the surface tension force.

behaviours [14]. The crossover means when an empirical parameter K

$$K = We^{0.5} Re^{0.25} \quad (30)$$

is smaller than a threshold value K_c , only deposition is observed. Otherwise, splashing develops.

In addition, the spread radius of splashing, r , was found to be expressed by a power law [12]:

$$r \cong \sqrt{DUt} \quad (31)$$

Though it is difficult to precisely decide the value of K_c , splashing occurs when the Reynolds number is large enough under a certain value of the Weber number. Following previous simulations [12], a serial of computations was performed in the range of the Reynolds numbers 20–500.

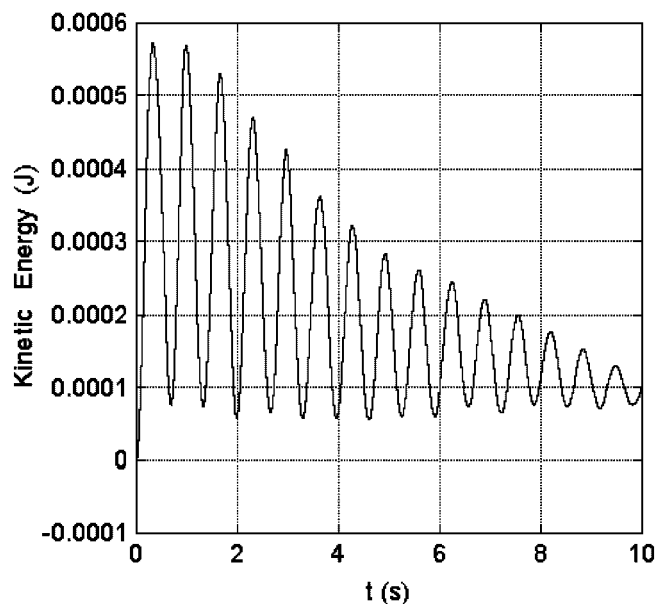


Figure 9. Transient kinetic energy for the square ethanol droplet oscillation.

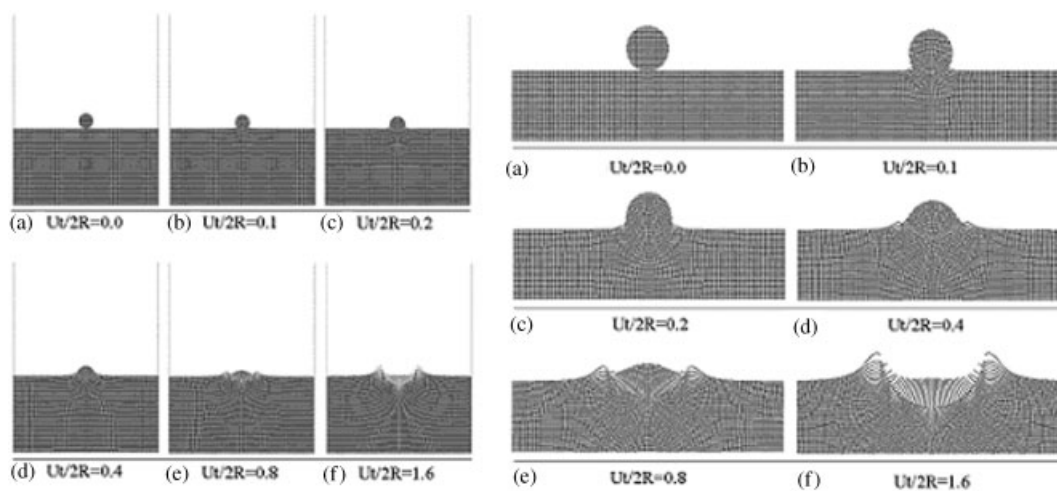


Figure 10. Time evolution of droplet deposition at $Re = 20$ and $We = 8000$ (the initial diameter and velocity of the droplet were 0.05 m and 40.0 m s^{-1} , respectively; the length and height of the liquid layer were 0.05 and 0.025 m , respectively; the length and height of the tank were 0.05 m . Simulation results in the left part of the figure are enlarged and showed in the right).

The Weber number was fixed as 8000. In the present two-dimensional simulations, the interface between liquid and gas was assumed as free surface and hence only liquid phase was considered. Same fluid properties were used for both the droplet and the liquid layer. In the simulations,

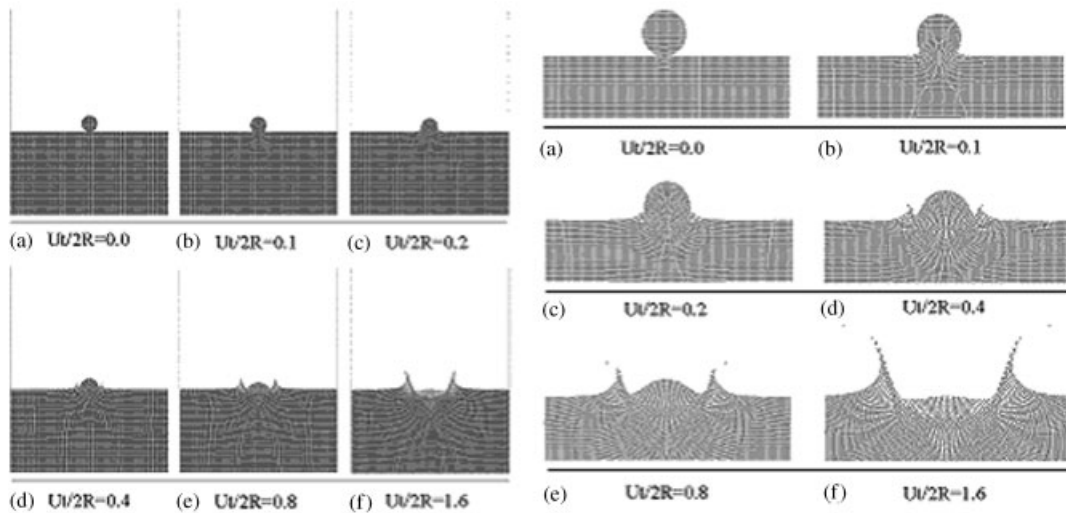


Figure 11. Time evolution of droplet splashing at $Re = 100$ and $We = 8000$ (the initial diameter and velocity were 0.0125 m and 8.0 m s^{-1} , respectively; the length and height of the liquid layer were 0.125 m and 0.625 m , respectively; the length and height of the tank were 0.125 m . Simulation results of the left part of the figure are enlarged and showed in the right).

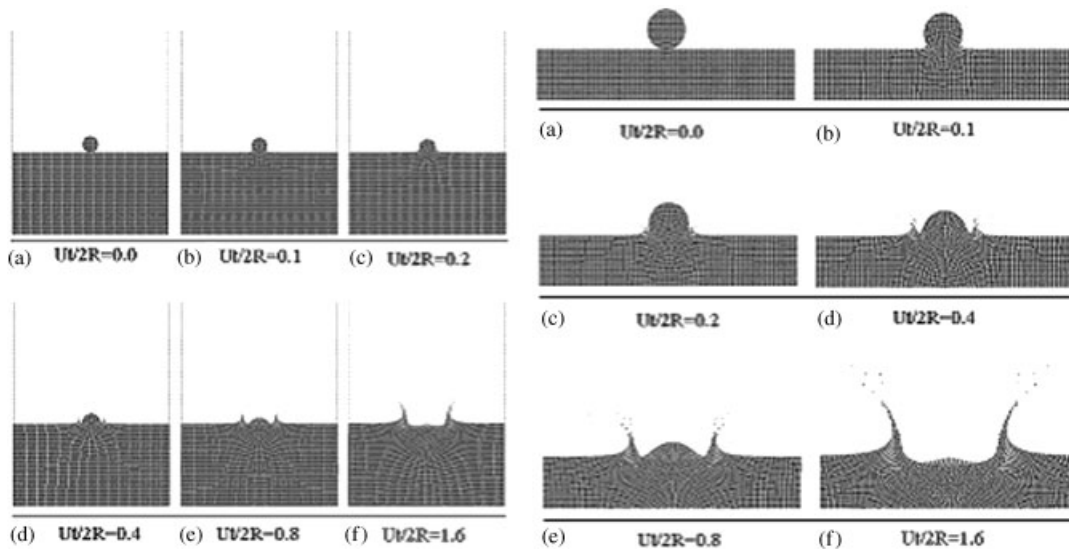


Figure 12. Time evolution of droplet splashing at $Re = 500$ and $We = 8000$ (the initial diameter and velocity of the droplet were 3.125 m and 1.6 m s^{-1} , respectively; the length and height of the liquid layer were 31.25 m and 15.625 m , respectively; the length and height of the tank were 31.25 m . Simulation results in the left part of the figure are enlarged and showed in the right).

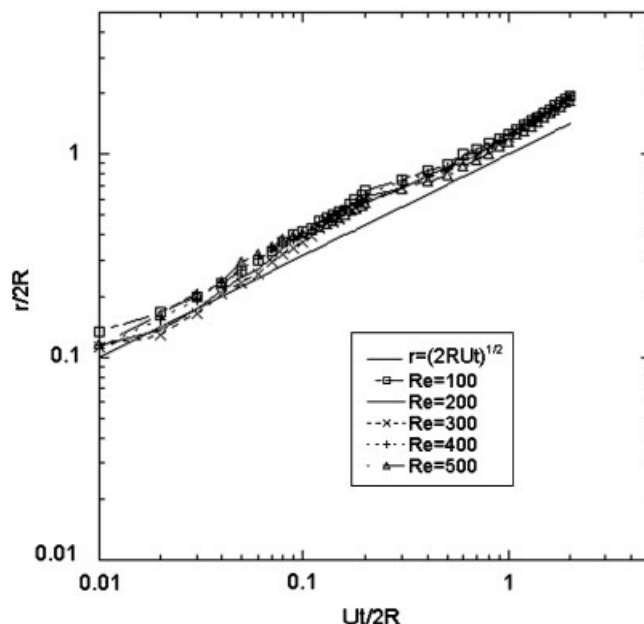


Figure 13. Log–log plot of the spread factor $r/2R$ as a function of non-dimensional time $Ut/2R$.

the density, surface tension coefficient and the dynamic viscosity were chosen as 1000 kg m^{-3} , 1.0 N m^{-1} and 10.0 kg ms^{-1} , respectively. The initial diameter and velocity of the droplet were calculated according to the different Reynolds number and the given Weber number. The length and depth of liquid layer were 10 and five times of the diameter of the droplet, respectively. The droplet was simulated by 1276 particles. The particle array of the liquid layer was 400×200 .

Simulation results are shown in Figures 10–13. Figures 10–12 indicate time evaluations of the droplet deposition or splashing phenomena at different Reynolds numbers. The development of the splashing spread radius at different Reynolds numbers is shown in Figure 13.

As can be seen in Figure 10, the deposition phenomenon was reproduced when the Reynolds and Weber numbers were 20 and 8000, respectively. In other cases, splashing phenomenon occurred as shown in Figures 11 and 12. The simulated deposition and splashing phenomenon agreed well with those obtained by the lattice Boltzmann method [12]. Figure 13 shows the spread radius changed as a function of non-dimensional time. The simulated results agreed with the power law, Equation (31).

5. CONCLUSION

In this study, a new algorithm for the surface tension model in moving particle methods was proposed to simulate free surface flow with the surface tension. The oscillatory behaviour of an ethanol droplet and the droplet impact into a liquid surface were successfully simulated using the FVP method with the proposed algorithm. The FVP simulation reproduced characteristics of the oscillatory droplet reasonably. The deposition and splashing phenomena in the droplet impact were successfully simulated with different Reynolds numbers. The simulated splashing spread radius

was in agreement with a power law. The present results show that the proposed algorithm can be applied in moving particle methods to simulate flow problems related with the surface tension force.

NOMENCLATURE

A	Overlapped volume between cell and particle (m^3)
d, D	spatial dimensions or diameter (m)
F	external volume force or driven force (m s^{-2})
h	height (m)
l, L	length (m)
m	fluid mass in one cell (kg)
n	unit normal of surface
p	pressure (Pa)
r	position vector (m)
R	radius of particle control volume (m)
r_e	cut-off radius of the kernel function
Re	Reynolds number
S	surface of particle control volume (m^2)
T	Temperature (K)
t	time (s)
u	velocity (m s^{-1})
V	control volume of particles (m^3)
W	Frequency (s^{-1})
We	Weber number

Greek letters

α	tuning parameter for the estimation of interaction between particles
ε	an arbitrary small number
$\theta, \hat{\theta}$	interaction parameter between particles
Φ	arbitrary scalar quantity
ρ	density (kg m^{-3})
ν	kinematic viscosity ($\text{m}^2 \text{s}^{-1}$)
Δl	initial distance between two particles (m)
ΔL	size of grid (m)
Δt	time step size (s)
σ	surface tension coefficient (N m^{-1})
μ	dynamic viscosity ($\text{kg m}^{-1} \text{s}^{-1}$)

Subscripts

i, j	particle number
--------	-----------------

Superscripts

*	temporal value
---	----------------

ACKNOWLEDGEMENTS

We would like to thank Prof. K. Yabushita for helpful suggestions and comments on the FVP method. One of the authors, Shuai Zhang, gratefully acknowledges support from Ministry of Education, Culture, Sports, Science and Technology, Japan by providing the MONBUKAGAKUSHO Scholarship.

REFERENCES

1. Brackbill JU, Kothe DB, Zemach C. A continuum method for modeling surface tension. *Journal of Computational Physics* 1992; **100**:335–354.
2. Morris JP. Simulating surface tension with smoothed particle hydrodynamics. *International Journal for Numerical Methods in Fluids* 2000; **33**:333–353.
3. Nomura K, Koshizuka S, Oka Y, Obata H. Numerical analysis of droplet breakup behaviour using particle method. *Journal of Nuclear Science and Engineering* 2001; **38**:1057–1064.
4. Liu J, Koshizuka S, Oka Y. A hybrid particle-mesh method for viscous, incompressible, multiphase flows. *Journal of Computational Physics* 2005; **202**:65–93.
5. Yabushita K, Hibi S. A finite volume particle method for an incompressible fluid flow. *Proceeding of Computational Engineering Conference* 2005; **10**:419–422 (in Japanese).
6. Rhoades CE. A fast algorithm for calculating particle interactions in smooth particle hydrodynamic simulations. *Computer Physics Communications* 1992; **70**:478–482.
7. Issa RI. Solution of the implicitly discretised fluid flow equations by operator-splitting. *Journal of Computational Physics* 1985; **62**:40–65.
8. Meijerink JA, Van Der Vorst HA. An iterative solution method for linear systems of which the coefficient matrix is a symmetric M-matrix. *Mathematics of Computation* 1977; **31**:148–162.
9. Williams MW, Kothe DB, Puckett EG. Accuracy and convergence of continuum surface tension models. *LA-UR-98-2268*.
10. Fyfe DE, Oran ES, Fritts MJ. Surface tension and viscosity with Lagrangian hydrodynamics on a triangular mesh. *Journal of Computational Physics* 1988; **76**:349–384.
11. Rein M. Phenomena of liquid drop impact on solid and liquid surfaces. *Fluid Dynamics Research* 1993; **12**:61–93.
12. Lee T, Lin C. A stable discretization of the lattice Boltzmann equation for simulation of incompressible two-phase flows at high density ratio. *Journal of Computational Physics* 2005; **206**:16–47.
13. Jossierand C, Zaleski S. Droplet splashing on a thin liquid film. *Physics of Fluids* 2003; **15**(6):1650–1657.
14. Mundo C, Sommerfeld M, Tropea C. Droplet-wall collisions: experimental studies of the deformation and breakup process. *International Journal of Multiphase Flow* 1995; **21**:151–173.